Transmission and reflection of internal wave beams

Kate D. Gregory and Bruce R. Sutherland[a)]
Department of Physics, University of Alberta, Edmonton, Alberta T6G 2G7, Canada

(Received 9 March 2010; accepted 7 August 2010; published online 8 October 2010)

An existing method for predicting the partial transmission of plane internal gravity waves across a weakly stratified region is adapted so as to predict the transmission of internal wave beams having finite horizontal and vertical extent. The results are compared with laboratory experiments in which internal waves generated by an oscillating cylinder are incident upon a mixed region of varying depth and stratification. The results are in good agreement except when the characteristic frequency of the beam is close to the minimum buoyancy frequency of the weakly stratified mixed region. In this case, the predicted transmission coefficient varies rapidly with frequency and so is sensitive to small measurement errors. Applications of this method to atmospheric and oceanic internal waves are discussed. © *2010 American Institute of Physics*. [doi:10.1063/1.3486613]

I. INTRODUCTION

Within a stratified fluid, internal waves propagate vertically as well as horizontally due to buoyancy forces. Thus they provide a means for the vertical transport of momentum and energy in the atmosphere and ocean. Knowing where the waves propagate is crucial to assess where they exert drag and where they mix upon breaking.

The trajectory of an internal wave is typically calculated using "ray tracing" techniques,[1,2] which assume that the waves have small amplitude and that the vertical wavelength of the waves is small compared to the scale of vertical variations of the background stratification and velocity fields. Heuristics based on ray theory predict that the waves completely reflect from a level where the (possibly Doppler-shifted) frequency equals the background buoyancy frequency and they asymptotically approach a critical level,[3] where the horizontal phase speed of the waves matches the background flow speed (or, equivalently, where the Doppler-shifted frequency is zero). Recently, a variety of studies have been performed to test the limits of these heuristics through the inclusion of nonsteady background flows,[4–7] large-amplitude effects,[8] and rapid variations of the background fields with height.[6,9–12] All of these are idealized studies in which an analytically prescribed plane wave or wave beam is incident upon an analytically prescribed background field. The question being addressed in this work is the robustness of the predictions to inevitable errors that result from uncertainties in the measured properties of the incident waves and background fields.

For simplicity both in theory and for comparison with experiment, we assume the background is stationary and its stratification varies only with height. Specifically, we focus on the process of tunneling[9] in which a vertically propagating internal wave is incident upon a finite-depth region of relatively weak stratification through which the wave partially transmits.

Internal wave tunneling has previously been investigated by Eckart[13] who considered the transfer of energy between two regions of locally enhanced stratification, as is the case of the main and seasonal thermoclines in the ocean. A similar study of the atmosphere[14] examined the energy transfer by internal waves between the stratosphere and the ionosphere. In these cases, tunneling resulted from the resonant transfer of energy between pairs of vertical modes in the system and, as a result, energy periodically transferred upward and then downward; the transfer was not unidirectional and so a transmission coefficient could not be defined as would be done, for example, in the study of electron tunneling across a potential barrier or photon tunneling across thin films.

Inspired by observations of internal wave propagation through the weakly stratified mesosphere,[15–17] Sutherland and Yewchuk[9] were the first to investigate unidirectional internal wave tunneling. In two idealized circumstances, they derived formulae for the transmission coefficient of plane internal waves passing through a background with piecewise-constant stratification. In that work, internal wave tunneling in a laboratory experiment was demonstrated but the theory developed was too idealized to allow direct comparison with the experiment results: the actual stratification was smooth, not piecewise-constant, and the incident waves were manifest as a beam, not a monochromatic plane wave. Since that time, a numerical method has been developed that predicts the transmission of internal waves through arbitrarily specified background profiles of stratification and velocity.[10] Given the horizontal wave number and frequency of an incident plane wave, the code directly integrates the Taylor–Goldstein equation to predict the relative amplitude and structure of the transmitted wave. In particular, for a plane wave propagating from strong to weak stratification, they found that the heuristic ray theory prediction was accurate if the transition distance between two stratified regions was larger than one sixth of the vertical wavelength of the transmitted waves.

In Sec. II, we extend this result by examining the sensitivity of the predicted transmission coefficient to the smoothness of a stratification profile prescribed as a finite-depth region of weak stratification surrounded by strongly stratified

a)Electronic mail: bruce.sutherland@ualberta.ca.

fluid. The corresponding analytic profiles of background density closely match the measured density profiles established in laboratory experiments. The experiments themselves are described in Sec. III. As well as the experimental setup, here we describe the image processing techniques used to measure nonintrusively the amplitude and structure of incident and transmitted wave beams emanating from an oscillating cylinder. The comparison between theory and experiments is made in Sec. IV. Here we show that under certain parameter regimes, the theoretical prediction is very sensitive to details of the background stratification and incident wave properties. The summary of results and implications for application to the study of wave propagation in the atmosphere and ocean are discussed in Sec. V.

II. THEORY

A. Equations of motion

The evolution of inviscid, two-dimensional, small-amplitude internal waves in nonuniformly stratified Boussinesq fluid is given by the partial differential equation

$$\left(\frac{\partial^2}{\partial x^2}+\frac{\partial^2}{\partial z^2}\right)\frac{\partial^2\psi}{\partial t^2}+N^2\frac{\partial^2\psi}{\partial x^2}=0. \tag{1}$$

Here

$$N^2=-\frac{g}{\rho_0}\frac{d\bar{\rho}}{dz} \tag{2}$$

is the squared buoyancy frequency, which depends on the rate of decrease of the background density $\bar{\rho}(z)$ with height, ρ_0 is the characteristic density of the fluid, and g is the acceleration of gravity. (In the atmosphere, N^2 is given in terms of the rate of increase of the background potential temperature, but this detail is physically inconsequential in the Boussinesq approximation.)

Equation (1) is cast in terms of the stream function ψ, which is implicitly defined in terms of the horizontal and vertical velocity fields by

$$(u,w)=\left(-\frac{\partial\psi}{\partial z},\frac{\partial\psi}{\partial x}\right). \tag{3}$$

Because the coefficients of Eq. (1) depend only on z, the equation can be Fourier transformed in x and t such that a single Fourier component has the form $\psi=\phi(z)\exp[i(kx-\omega t)]$, in which it is understood that the actual stream function is the real part of this expression and the complex-valued stream function amplitude $\phi(z)$ describes the vertical structure of a wave with horizontal wave number k and frequency ω. Explicitly, through substituting this expression into Eq. (1), ϕ is given by the solution of

$$\phi''+k^2\left(\frac{N^2}{\omega^2}-1\right)\phi=0. \tag{4}$$

This is a special case of the Taylor–Goldstein equation[18] in which there is no background flow. As expected, solutions to Eq. (4) are oscillatory in z, where $\omega<N(z)$, and exponential in z, where $\omega>N(z)$. The precise determination of ϕ depends on the upper and lower boundary conditions as well as the prescription of N.

Given ϕ, one can go on to determine other fields of interest. In this study, two fields are of particular importance. The vertical displacement field ξ is related to the stream function by Eq. (3) and the condition $\partial_t\xi=w$. Thus in a uniformly stratified fluid, a vertically propagating plane wave with stream function amplitude A_ψ has vertical displacement amplitude

$$A_\xi=-\frac{k}{\omega}A_\psi=-\frac{k}{N\cos\Theta}A_\psi. \tag{5}$$

In the laboratory experiments, we directly measure the time rate of change of the squared buoyancy frequency due to the stretching and compression of isopycnals by waves

$$N_t^2=-\frac{g}{\rho_0}\frac{\partial^2\rho}{\partial t\,\partial z}\simeq -N^2\frac{\partial^2\xi}{\partial t\,\partial z}. \tag{6}$$

The second expression makes use of the fact that if the isopycnal displacements are small, the fluctuation density field ρ is related to the vertical displacement field by $\rho=-\bar{\rho}'\xi$, in which $\bar{\rho}'$ is the background density gradient. In terms of the stream function and vertical displacement field, the amplitude of N_t^2 is

$$A_{N_t^2}=k^2N^2\tan\Theta A_\psi=-kN^3\sin\Theta A_\xi. \tag{7}$$

In these expressions, we have defined

$$|\Theta|=\cos^{-1}(\omega/N), \tag{8}$$

which is the angle formed by lines of constant phase to the vertical. Equivalently, from the dispersion relation for internal waves, $\Theta=\tan^{-1}(m/k)$, where m is the vertical wave number. In this last expression, the sign of Θ is determined by the sign of m/k. In particular, waves with their group velocity oriented downward and rightward have m and k both positive.

Although Eqs. (5) and (7) have been derived for plane waves in uniformly stratified fluid, they can be used to estimate the relative amplitude of the waves in regions where the fluid is approximately uniformly stratified.

B. Transmission coefficients

Equation (4) can be solved analytically for piecewise-constant profiles of N^2. Arbitrarily supposing the wave is incident from above with stream function amplitude $A_{\psi I}$ and that it partially reflects with amplitude $A_{\psi R}$ and transmits with amplitude $A_{\psi T}$, matching conditions requiring ϕ and its derivative to be continuous, where N^2 discontinuously jumps, give formulae separately relating $A_{\psi R}$ and $A_{\psi T}$ to $A_{\psi I}$. In particular, for waves transmitting from one region of constant N to another, the polarization relation (5) can then be used to relate the reflected and transmitted vertical displacement amplitudes to that of the incident wave amplitude. From these, one can find relative energy flux associated with the reflected and transmitted waves. Explicitly, the horizontally averaged energy flux given in terms of the vertical displacement amplitude is

$$\langle F_E \rangle = \tfrac{1}{2} N^2 |A_\xi|^2 c_{gz}, \tag{9}$$

in which $c_{gz}=(N/k)\cos^2\Theta \sin\Theta$ is the vertical group velocity. If the buoyancy frequency in the transmitted region is the same as that in the incident region (as is the case in the experiments examined here), the ratio of transmitted to incident wave energy flux gives the transmission coefficient

$$T = \frac{\frac{1}{2}\frac{N^3}{k}\cos^2\Theta \sin\Theta |A_{\xi T}|^2}{\frac{1}{2}\frac{N^3}{k}\cos^2\Theta \sin\Theta |A_{\xi I}|^2} = \left|\frac{A_{\xi T}}{A_{\xi I}}\right|^2. \tag{10}$$

Likewise, the reflection coefficient is defined by

$$R = \left|\frac{A_{\xi R}}{A_{\xi I}}\right|^2. \tag{11}$$

It can be independently checked that $T+R=1$, as required by energy conservation. In the presence of background shear, the appropriate analogous definition of T is the ratio of transmitted to incident flux of wave action.[8] This reduces to the definition (10) for uniform or zero flow. Note that when dealing with incident plane waves, the polarization relations (7) show that it is irrelevant whether the amplitudes in Eq. (10) are those of stream function, vertical displacement, or N_t^2.

In particular, for plane internal waves incident upon an N^2-barrier prescribed by

$$N^2 = \begin{cases} N_0^2, & |z| > L/2, \\ 0, & |z| \le L/2, \end{cases} \tag{12}$$

the transmission coefficient is[9]

$$T = \left\{1 + \left[\frac{\sinh(kL)}{\sin(2\Theta)}\right]^2\right\}^{-1}. \tag{13}$$

The numerical solution method of Eq. (4) for any prescribed $N^2(z)$ was developed by Nault and Sutherland.[10] The incident waves were assumed to be horizontally periodic with given horizontal wave number k and with fixed frequency ω. In terms of the stream function amplitude of the incident waves $A_{\psi I}$, the code finds the amplitudes of the transmitted and reflected waves $A_{\psi T}$ and $A_{\psi R}$, respectively.

Here we use this code to examine the effect of smooth transitions from strong to weak stratification as measured in laboratory experiments. To this end we examine the transmission of plane waves across an N^2 profile given by

$$N^2 = N_0^2 + \frac{N_0^2 - N_1^2}{2} \times \left[\tanh\left(\frac{z-z_u}{\sigma_u}\right) - \tanh\left(\frac{z-z_l}{\sigma_l}\right)\right]. \tag{14}$$

Here, the parameters σ_u and σ_l represent half the distance over which N^2 changes from one stratification to another. In the laboratory experiments presented here, the symmetry of the way in which we establish a nonuniformly stratified ambient gives $\sigma_u \simeq \sigma_l$. We denote this transition distance simply by σ. Likewise, N_0 is the buoyancy frequency of the upper and lower strongly stratified regions and for sufficiently small σ, N_1 is the buoyancy frequency of the middle weakly stratified region. The values z_u and z_l denote the top and bottom, respectively, of the weakly stratified region occurring at the inflection points of $N^2(z)$. In the limit $\sigma \to 0$ and with $N_1=0$, Eq. (14) reduces to the piecewise-constant formula (12) in which $z_u=L/2$ and $z_l=-L/2$. Using the Taylor–Goldstein solver with very small σ and comparing the resulting transmission coefficients with those predicted by the analytic formula (13), we find excellent agreement for a wide range of k and ω values. This check on the code allows us to proceed with confidence in using it to predict transmission across arbitrary, smoothly varying N^2 profiles.

Figure 1 compares transmission coefficients as a function of k and ω for internal waves propagating through background stratification given by Eq. (14) with $z_u=L/2$, $z_l=-L/2$, $N_1^2/N_0^2=0$, and $\sigma_u=\sigma_l=\sigma$. The plot for the approximately piecewise-constant profile is generated using $\sigma/L \simeq 0$ (the actual value being at the vertical resolution of the code $\Delta z=0.01L$) and the plot for the smooth analytic profile is generated using $\sigma/L=0.1$. The latter relative interface thickness was chosen to be sufficiently large to introduce an obvious smooth transition in N^2 while still being small enough that $N^2(0)=0$, as shown in the sketch to the right of Fig. 1(b).

The resulting plots are similar both qualitatively and quantitatively. In both cases, for fixed k, transmission coefficients are greatest if $\omega=N_0/\sqrt{2}$, which corresponds to wave propagation in the strongly stratified region moving in a direction from the vertical of $\Theta \approx 45°$. For fixed ω, transmission decreases as kL becomes large corresponding to increasing depth of the mixed region relative to k^{-1}.

Discrepancies between the two transmission plots can be seen more clearly by subtracting the two plots, as shown in Fig. 1(c). Differences on the order of 10% are seen for very small values of ω/N_0 due to the change in σ/L; otherwise, the difference in transmission is negligible. The transmission coefficient has also been computed for $\sigma/L=0.2$ (not shown) and the difference between this and the $\sigma/L=0.0$ case is given in Fig. 1(d). Doubling σ gives substantially larger transmission for small ω/N_0 with little change noted for significantly nonhydrostatic waves. For this relatively large value of σ/L, the actual minimum value of the N^2 profile is $N_{\min} \simeq 0.14 N_0$. So waves do not become evanescent if their frequency is smaller than $N_{\min}$. This explains why low frequency waves transmit more effectively as σ increases.

Even if ω is moderately larger than $N_{\min}$, enhanced transmission occurs in part because the effective depth of the evanescent region is reduced. For example, consider incident waves with frequency $\omega=0.2N_0$ and horizontal wave number $k=1.0/L$. With $\sigma=0.2L$, the distance over which the waves are evanescent is $L_{\text{eff}} \simeq 0.36L$ and their computed transmission coefficient is $T=0.276$. The corresponding transmission coefficient for these waves crossing the piecewise-constant N^2 profile having $\sigma=0$ is $T=0.100$, but with $kL_{\text{eff}}=0.36$ it is $T_{\text{eff}}=0.53$. Computing the transmission coefficient for waves with $\omega=0.2N_0$ and $kL=0.36$ that cross a piecewise-constant N^2 profile having $N_1=0.14N_0$ gives a similar value: $T=0.54$. Thus, with $\omega > N_{\min}$, it is primarily the effective depth of the evanescent region that determines their enhanced transmission. If ω is moderately larger than $N_{\min}$, the depth is small. If ω is moderately smaller than N_0, the depth is close to L.

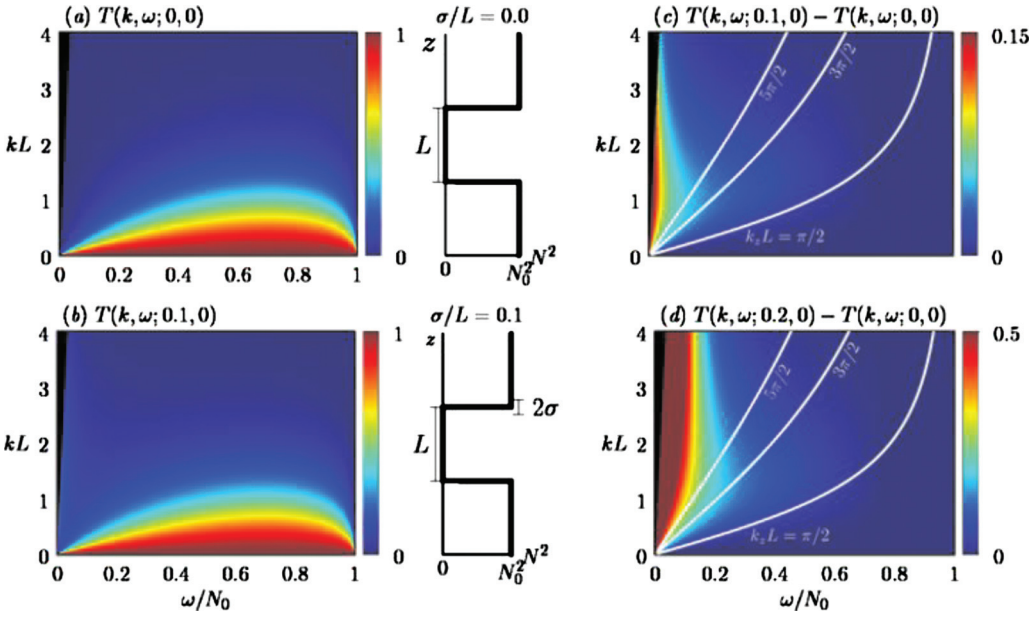

FIG. 1. (Color) Plots of the transmission coefficient $T(k,\omega;\sigma/L,N_1^2/N_0^2)$ for tunneling across an unstratified layer. The background N^2 profile is given by Eq. (14) with $N_1=0$ and transition depth $\sigma_u=\sigma_l\equiv\sigma$ prescribed such that (a) $\sigma/L\simeq 0.0$ and (b) $\sigma/L=0.1$. The corresponding N^2 profiles are shown to the right of both plots. The difference in transmission coefficients between the $\sigma/L=0.1$ and 0.0 cases and between the $\sigma/L=0.2$ and 0.0 cases is given in (c) and (d), respectively. (Note the different color scales in these figures.) The superimposed white lines on (c) and (d) are plots of kL vs ω/N_0 for constant $k_zL=\pi/2$, $3\pi/2$, and $5\pi/2$, as indicated. The code used to compute T is inaccurate where ω is very small and is blacked out in this region of parameter space.

So transmission is enhanced with $\sigma>0$, but the relationship between T and the effective depth of the tunneling region particularly for incident waves with horizontal wave numbers $k\simeq 1/L$ is nontrivial. The dispersion relation for internal waves in fluid with buoyancy frequency N_0 gives kL as a function of ω/N_0 for given relative vertical wave number k_zL. This is plotted as the superimposed white lines in Figs. 1(c) and 1(d) for $k_zL=\pi/2$, $3\pi/2$, and $5\pi/2$. The curves show no correlations between enhanced transmission with the vertical wave number relative to σ, though we show next that transmission is enhanced in proximity to these curves if $N_1>0$ and $\omega<N_1$.

We next consider the circumstance in which the middle region is weakly stratified instead of well-mixed. This situation corresponds more closely to the atmosphere, in which the mesosphere is bounded by the relatively strongly stratified stratosphere and ionosphere and it is representative of the ocean where the seasonal and main thermoclines straddle relatively weakly stratified water. It is also the circumstance of the laboratory experiments we report here.

Figure 2 examines transmission through an N^2 profile with $z_u=L/2$, $z_l=-L/2$, $N_1^2/N_0^2=0.5$, and $\sigma_u=\sigma_l=\sigma$. As above, it compares transmission coefficients through an approximately piecewise-constant profile with $\sigma/L=0.01$, 0.1, and 0.2.

In Figs. 2(a) and 2(b), there are now two distinct transmission regimes: one with $0<\omega<N_1$ and one with $N_1<\omega<N_0$. In the latter case, the plot exhibits similar behavior as in Fig. 1: for fixed ω, transmission drops off as kL increases. However, if $\omega<N_1$, transmission remains large for all kL because the wave frequency is smaller everywhere than the background buoyancy frequency. The banded pattern in this range is due to the resonance of plane waves within the weakly stratified region occurring if the vertical wave number of the plane wave in the weakly stratified region is approximately an integer multiple of π/L.[9,19] If σ is nonnegligible, transmission is enhanced in this banded region because the depth of the weakly stratified region is not as precisely given by L, allowing a greater range of plane waves to be resonant. The difference in transmission rates between the $\sigma/L=0.1$ and 0.0 cases and between the $\sigma/L=0.2$ and 0.0 cases is shown explicitly in Figs. 2(c) and 2(d). As in the case with $N_1=0$, increasing σ increases the difference but does not substantially change the qualitative structure of the plot. That the constant-k_zL curves somewhat follow the constant contours of enhanced transmission is a consequence of the resonance condition whereby an approximately integer multiple of half-vertical-wavelengths span the depth of the weakly stratified region.

Between the two regimes, where $\omega\simeq N_1\simeq N_{\min}$, the transmission changes rapidly with ω for $kL\gtrsim 2$. We will refer to this as the "transition region." For incident waves having frequencies and horizontal wave numbers in the transition region, uncertainties in ω or N_1 lead to large uncertainties in the transmission coefficient.

C. Wave beam transmission

So far we have examined the theory for transmission of plane waves. We will now extend this theory to that for wave beams which are monochromatic in time but horizontally localized in space. Assuming the waves are small-amplitude, we can use the fact that wave beams are a superposition of plane waves to do this. Here we will consider the transmission of a wave beam having fixed frequency but which is horizontally localized, as is the case of waves generated from

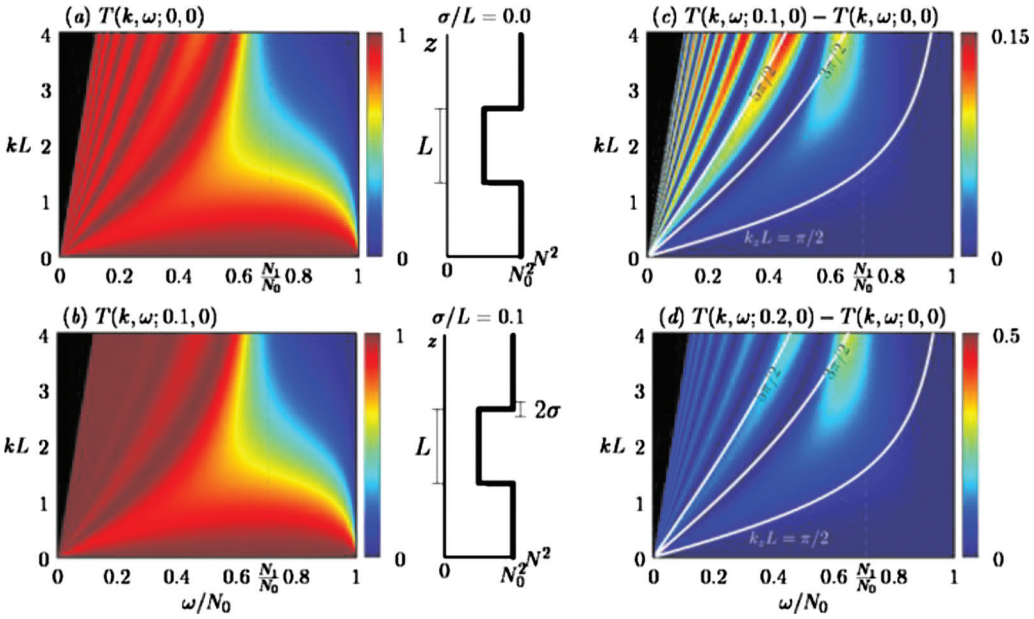

FIG. 2. (Color) As in Fig. 1 but showing plots of transmission coefficient computed for tunneling across a weakly stratified region in which $N_1^2/N_0^2=0.5$ and with (a) $\sigma/L \simeq 0.0$ and (b) $\sigma/L=0.1$. The difference in transmission coefficients between $\sigma/L=0.1$ and 0.0 case and between $\sigma/L=0.2$ and 0.0 cases is given in (c) and (d), respectively. In each plot the vertical dashed lines indicate values of $\omega=N_1$.

a cylinder oscillating at fixed frequency. The approach is similar to the Fourier transform approach of Kistovich and Chashechkin[20] and of Mathur and Peacock,[12] except that here we require the horizontal extent of our domain to be finite, and so we cast our formula as a Fourier series.

When dealing with wave beams, as opposed to plane waves, the expressions for the transmission coefficients now depend on what field is used to describe the amplitude of the incident and transmitted waves. In particular, by forming a Fourier series of the vertical displacement field ξ of the incident waves at a horizontal location prior to reaching the mixed region, the vertical displacement amplitudes $A_{\xi n}$ of waves with horizontal wave number k_n are determined. Here, $k_n=n2\pi/L_x$ is the wave number of the nth mode in a domain of horizontal extent L_x. The energy flux of each plane wave component of the incident wave beam is given by Eq. (9) with $A_\xi \rightarrow A_{\xi n}$. Using Eq. (10), we can then predict the energy flux of the corresponding transmitted plane wave component where the transmission coefficients are calculated numerically for each k_n and fixed ω.

The transmission coefficient compares the total energy flux of the waves having passed through the mixed region to the total energy flux of the incident waves

$$T_{\text{thy}} = \frac{\sum_n \frac{N^3}{2k_n}\cos^2\Theta \sin\Theta |A_{\xi n}|^2 T_n}{\sum_n \frac{N^3}{2k_n}\cos^2\Theta \sin\Theta |A_{\xi n}|^2} = \frac{\sum_n \frac{1}{k_n}|A_{\xi n}|^2 T_n}{\sum_n \frac{1}{k_n}|A_{\xi n}|^2}. \tag{15}$$

Here, T_n is the transmission coefficient for plane waves with horizontal wave number k_n. In the last expression we have used the fact that ω (and hence Θ) is the same for all wave components.

For the purposes of comparison with experiments, we characterize the wave structure in terms of the time rate of change of the perturbed squared buoyancy frequency given by Eq. (6). By composing a Fourier series of N_t^2 in the horizontal x-dimension, we have, in terms of the discrete horizontal wave number k_n, that

$$N_t^2 = \sum_{n=-\mathcal{N}}^{\mathcal{N}} \frac{1}{2} A_n e^{ik_n x}, \tag{16}$$

in which we have used the notation $A_n \equiv A_{N_t^2 n}$ to represent the amplitude of the nth mode of the N_t^2 field which has wave number k_n. The maximum mode number N is set so that $\lambda_{\mathcal{N}} \equiv 2\pi/k_{\mathcal{N}} = L_x/\mathcal{N}$ is much smaller than the observed characteristic length scale of the wave beam. The complex amplitude A_n has magnitude equal to the half-peak-to-peak amplitude of the N_t^2 field corresponding to the nth mode. To ensure the field is real, $A_{-n}=A_n^*$, in which the star denotes complex conjugate.

Equation (7) relates the amplitude of the vertical displacement field to the amplitude of the N_t^2 field for plane waves. Combining this with Eq. (15), the transmission coefficient defined in terms of amplitudes of the N_t^2 field is

$$T_{\text{thy}} = \frac{\sum_n \frac{1}{k_n^2}|A_n|^2 T_n}{\sum_n \frac{1}{k_n^2}|A_n|^2}. \tag{17}$$

III. EXPERIMENT METHODS

A. Experiment setup

Experiments were performed in a glass tank 197 cm in length, 20 cm in width, and 50 cm in height. The tank was filled to a depth of either 30 or 45 cm with salt-stratified fluid using the standard "double bucket" technique.[21] The stratifi-

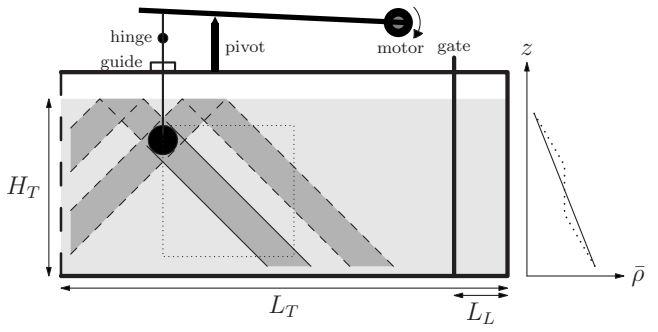

FIG. 3. Front view of the experimental setup for the oscillating cylinder experiments. A circular cylinder is vertically oscillated using a motor. A camera is positioned with its field of view (dotted box) including the primary beam propagating downward and to the right (solid lines). The surface-reflected beams and the beams traveling to the left of the cylinder are not of significance here, as indicated by the long dashed lines. The solid line in the graph on the right shows the density profile of uniformly stratified fluid and the dotted line shows the profile after mixing at mid-depth by the passage of an intrusive gravity current.

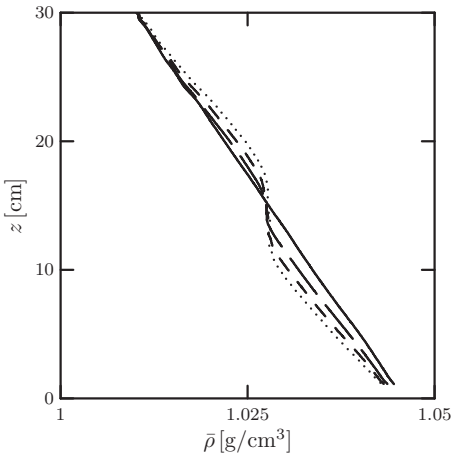

FIG. 4. Four density profiles measured after successive intrusions in one set of experiments. The solid line plots the uniform stratification created by using the double bucket method. The long dashed, short dashed, and dotted lines plot the density profiles created after repeated intrusions were released at mid-depth causing the depth of the mixed layer to increase.

cation was established such that the density at the bottom of the tank was approximately 1.05 g/cm^3 and the density at the top of the tank was approximately 1.00 g/cm^3. A front view schematic of the tank is shown in Fig. 3.

A conductivity probe was used to measure the background density field $\bar{\rho}(z)$. The vertically traversing probe directly measures voltage approximately 56 times/cm and, interpolating from the calibration solutions, these were converted to densities.

Internal waves were produced by a vertically oscillating circular cylinder.[22] In different experiments, one of two circular cylinders were used having radii $R=1.0$ cm and $R=2.4$ cm. The cylinder was attached to a vertical rod suspended from a main arm which in turn was attached to the oscillating motor, as shown in Fig. 3. A pivot was used to steady the main arm and a guide near the top of the rod was used to keep its oscillations vertical. The cylinder was positioned near the top left side of the field of view so that the beam traveling right and downward (the primary beam) could be viewed clearly by the camera. The cylinder was placed sufficiently below the surface so that the right and upward-propagating beam did not interfere significantly with the primary beam upon reflection from the surface. The two beams generated to the left of the cylinder were able to propagate freely to the far left end of the tank and did not interfere with the primary beam. The waves were generated with frequency ω equal to the cylinder oscillation frequency ω_c and the angle Θ to the vertical formed by the cross-pattern of wave beams was set by the frequency relative to N through the relation (8). The range of frequencies examined was restricted to $0.3<\omega_c/N_0<0.5$. Experiments with $\omega_c/N_0<0.3$ produced a primary beam whose angle to the vertical was so large ($\Theta \gtrsim 70°$) that the transmitted beam was outside the camera's field of view. Experiments with $\omega_c/N_0>0.5$ produced an upward-propagating beam emanating from the cylinder which reflected off the surface and interfered significantly with the primary beam.

The rate of dissipation due to viscosity is estimated by νR^{-2}, in which it is assumed the cross-beam wavelength scales with the cylinder radius R.[23–25] In these experiments, the dissipation rate ranges from 0.01 to 0.002 s^{-1}. So the time for significant loss of energy due to viscosity is on the order of 100 and 500 s for small and large cylinder experiments, respectively. In comparison, the vertical group velocity [given below Eq. (9)] is on the order of 1 cm/s consistent with our observation that the wave beam reaches steady state from the top to bottom of the domain after approximately 30 s. The time to pass from the top to the bottom of the tunneling region over a distance less than 10 cm is therefore significantly shorter than the viscous dissipation time. For this reason, viscosity is not expected to play a significant role in the wave dynamics.

In our examination of internal wave propagation in nonuniformly stratified fluid, we specifically studied the transmission of a wave beam through a relatively weakly stratified layer at mid-depth in the tank. The method of creating this weakly stratified region follows the procedure by Sutherland.[26] A gate is inserted on the right side of the tank a distance of $L_L=18.5$ cm or 14.5 cm from the right wall and the fluid in the lock behind the gate is mixed thoroughly (see Fig. 3). The gate was then quickly vertically removed releasing an intrusive gravity current that propagated horizontally into the ambient stratified fluid at mid-depth. After the system became stationary once more, the process had created a region of weakly stratified fluid between 3 and 4 cm depth. For successive experimental runs the procedure was repeated, broadening the depth of the mixed region and decreasing its minimum stratification. Each experiment has four or more runs with the first run always being with uniformly stratified fluid. The background density profile $\bar{\rho}(z)$ is measured before and after each run of the experiment. Examples of density profiles taken after successive runs of one set of experiments are shown in Fig. 4.

Each nonuniform density profile is then empirically fit to a smooth analytic formula of the following form:

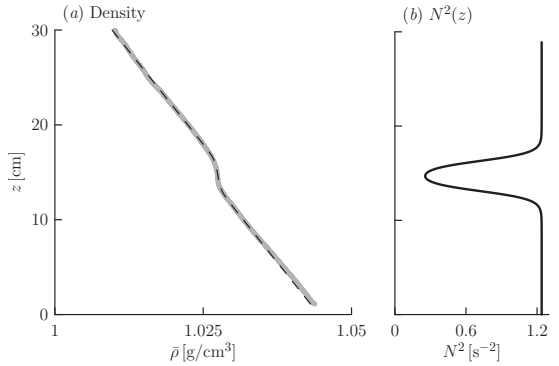

FIG. 5. (a) Background density and (b) N^2 profiles for oscillating cylinder experiment 1b. In (a), the thick gray line is the experimental background density profile and the dashed black line is its best-fit analytic curve.

$$\bar{\rho}(z) = \rho_0 + \left(\frac{\rho_0}{g}\right)(z_{\max} - z)N_0^2 - \left(\frac{\rho_0}{2g}\right)(N_0^2 - N_1^2) \times \left[\sigma_u \mathrm{LC}\left(\frac{z - z_u}{\sigma_u}\right) - \sigma_l \mathrm{LC}\left(\frac{z - z_l}{\sigma_l}\right) + z_u - z_l\right]. \quad (18)$$

Here, for brevity, we have defined $\mathrm{LC}(Z) = \ln[\cosh(Z)]$, functions that were chosen because their structure formed a good fit to the experimental profiles. Using Eq. (2), the density profile (18) corresponds to the squared buoyancy frequency given by Eq. (14).

The points of maximum curvature at the edges of the mixed region were used to find z_u and z_l. N_0 and N_1 were found from the slope of the best-fit lines to their respective regions of the density profile. By symmetry of the way in which the mixed region was formed, we assume the upper and lower stratifications were the same and also that $\sigma_u = \sigma_l = \sigma$. These parameters were found from density profiles before and after and experiment and the resulting pair of density profiles were averaged.

Figure 5(a) shows the measured density profile and the analytic fit to it, taken from an experiment after a single intrusion has partially mixed the tank at mid-depth. The resulting parameters were found to be $N_0 = 1.11$ s^{-1}, $N_1 = 0.43$ s^{-1}, $z_u = -8.20$ cm, $z_l = -11.40$ cm, $\sigma = 0.90$ cm, and $\rho_0 = 1.01$ g/cm^3. With these parameters, the corresponding N^2 profile (14) is determined as shown in Fig. 5(b).

Note that the actual minimum of N, $N_{\min}$, is significantly larger than N_1 if $\sigma \gtrsim 0.2L$. And so we expect the resulting slope of the density profile at mid-depth to be larger in magnitude than the measured slope, which was used to find N_1. However, comparing the analytic density profile to measurements [as in Fig. 5(a)], the difference in slopes is hardly distinguishable by eye. Separately we have performed a regression analysis in an attempt to determine optimal values of N_1, σ, z_l, and z_u that fit the measured density profile. However, we found no clear convergence to a unique set of these variables. Of course due to significantly noisier *in situ* observations of the atmosphere and ocean and due to extrapolation of observations from the location of observed profiles to internal wave propagation sites of interest, clearly identifying the minimum in the N^2 profile would be more challenging in practice. As a way to emphasize the uncertainty in determining the actual value of N at mid-depth, in our analysis of results we use the difference of $N_{\min}$ and N_1 as an objective estimate of the error in the measurement of N in the weakly stratified region. Given the empirically determined N^2 profile, we can then predict the transmission coefficient for waves of given frequency and horizontal wave number. These predictions are sensitive to the actual minimum value of N^2 for waves in the transition region.

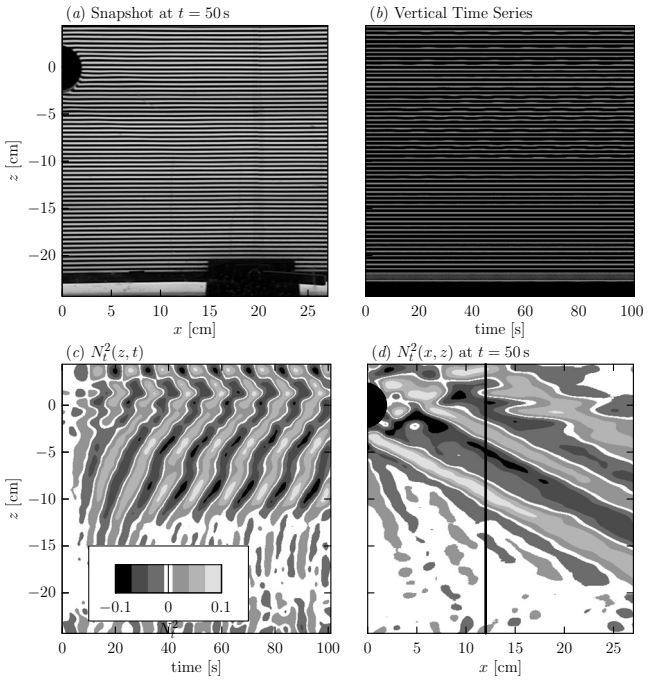

FIG. 6. (a) A snapshot taken from an experiment $t = 50$ s after the cylinder centered at the origin begins oscillating. (b) A vertical time series taken 12 cm to the right of the center of the cylinder, (c) its processed N_t^2 vertical time series, and (d) a snapshot of the processed N_t^2 field. The vertical line in (d) indicates the location of the vertical time series. The N_t^2 field ranges from -0.1 to 0.1 s^{-3} with the grayscale indicated in (c). In this experiment, the stratification is uniform (N^2 constant) so the primary beam propagates at a constant angle to the vertical from the upper-left to the lower-right corner of the image. The surface-reflected beam is evident above the primary beam. In this experiment, $N_0 = 1.08$ s^{-1} and $\omega_c = 0.50$ s^{-1}.

B. Synthetic schlieren technique

In order to measure the properties of internal waves in the tank, the two-dimensional synthetic schlieren method was used.[25] In our application, we placed an image of horizontal black and white lines behind the tank and illuminated it from behind with a bank of fluorescent tubes. Internal waves cause isopycnals alternately to compress together and to stretch apart. The corresponding refractive index changes cause the path of light traveling through the tank from the image to the camera to deflect. Thus the camera records an apparent distortion of the image from which the corresponding changes to the density gradient in the tank may be measured nonintrusively. The procedure is illustrated in Fig. 6.

A camera recording at 30 frames per second was placed approximately 280 cm in front of the tank. The camera's field of view was the region to the right and below the cylinder producing an image measuring approximately 30 cm

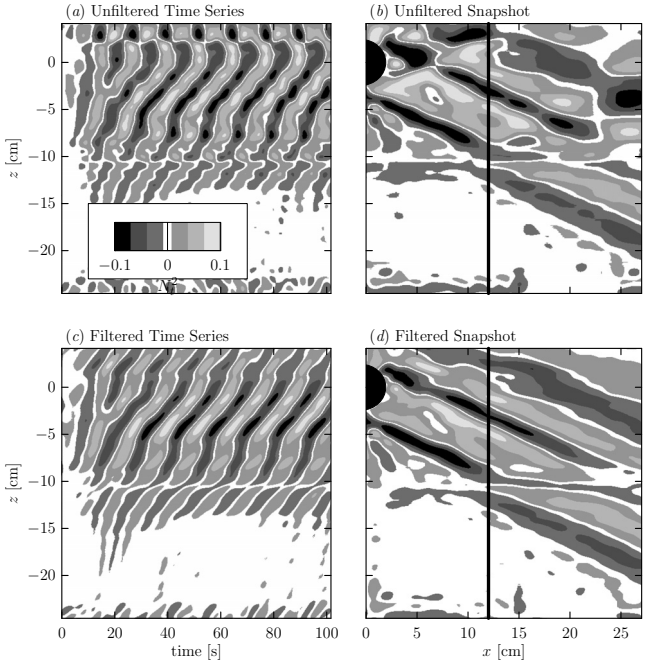

FIG. 7. (a) Vertical time series of the N_t^2 field taken at $x=12.01$ cm from the center of the cylinder and (b) the snapshot image of this field at time $t=50$ s. (c) The Hilbert transform is applied to the time series to filter out signals with negative vertical wave number (upward-propagating waves). (d) The corresponding filtered snapshot image. Vertical black lines in (b) and (d) indicate the position at which slices are taken to construct the vertical time series in (a) and (c), respectively. The images are taken from experiment 1b with corresponding density and N^2 profiles shown in Fig. 5. In all four frames, the N_t^2 field ranges from -0.1 to 0.1 s^{-3} as indicated by the inset grayscale in (a).

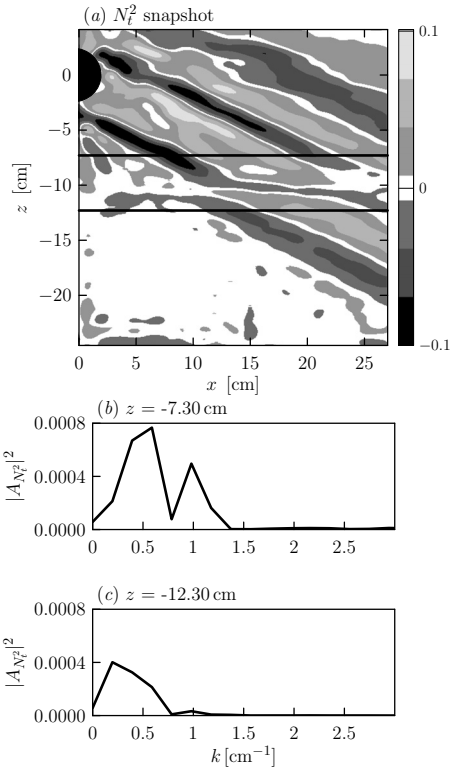

FIG. 8. (a) The Hilbert-filtered snapshot also shown in Fig. 7(d) but here with horizontal lines indicating levels at which the structure of incident and transmitted waves are computed. The field ranges from -0.1 to 0.1 s^{-3} as indicated by the grayscale to the right. The power associated with the Fourier series amplitudes computed from the N_t^2 field along a horizontal slice taken (b) above the weakly stratified region and (c) below it as indicated by the values of z in the plot label.

$\times 30$ cm. The resolution was approximately 15 pixels/cm in both spatial directions. Figure 6(a) shows a snapshot taken 50 s after the cylinder started to oscillate. The apparent displacement of the black and white lines behind the tank is only barely discernible by eye near the cylinder itself (which is centered at the origin). The digital camera can record intensity changes not discernible by eye, effectively monitoring displacements as small as 1/30th of the pixel extent, or about 0.002 cm.

In practice, a sequence was constructed of vertical time series spaced horizontally by 1 cm. From these we accurately measured the frequency of the oscillating wave generator and confirmed that waves were generated with the same frequency. The apparent rate of displacement of the image of lines is proportional to the time rate of change of the squared buoyancy frequency due to waves (N_t^2). Working with this field has the effect of removing long timescale changes within the tank. Amalgamating the resulting vertical time series, a snapshot of the N_t^2 field can be constructed at any time.

C. The Hilbert transform

In general, the Hilbert transform takes a function and shifts its phase by 90°, thus putting a real function into the complex plane. Previous studies have used the Hilbert transform on roll waves and hydrothermal traveling waves to demodulate the signal.[27,28] It has recently been applied to internal gravity waves as a technique for separating the four wave beams emanating from an oscillating source.[29] As in that work, we use the Hilbert transform to separate upward from downward-propagating waves in a vertical time series.

Figure 7 shows an example of applying the Hilbert transform to data from a laboratory experiment in which internal waves generated by an oscillating cylinder partially transmit through a weakly stratified region. A vertical time series image and a snapshot of the N_t^2 field taken after four buoyancy periods (time $\simeq 50$ s) is shown in Figs. 7(a) and 7(b). The corresponding Hilbert transform-filtered images are shown in Figs. 7(c) and 7(d), the filtering performed to reveal only the downward-propagating waves.

For the purposes of studying internal wave transmission, we keep only waves with positive vertical wave number thereby filtering out upward-propagating beams. This means that the part of the primary beam that reflects off the mixed region is removed as well as the transmitted beam after it reflects off the bottom of the tank.

D. Comparing theory with experiments

Once the measured N_t^2 field is filtered by the Hilbert transform to extract only downward-propagating waves, we are able to measure the structure of the incident wave beam independent of the reflected beam. From this, together with the measured structure of $N^2(z)$, we may use Eq. (17) to

TABLE I. Table of parameters and predicted and computed transmission coefficients for six sets of experiments. Within each set, the depth of the mixed region, measured by L, increases. The error estimates in the measurement of ω_c, N_0, σ, and L are shown in the second line of the table. Values of N_1 computed from the measured slope of the density profile at mid-depth underestimate the minimum value of the analytic profile for N given by Eq. (14). The value of $N_{\min}$ is greater by the amount shown in parentheses. The difference between T_{obs} and T_{thy} is greatest if ω_c/N_1 is sufficiently close to unity and the error in N_1 is sufficiently large.

Expt.	ω_c (s^{-1})	N_0 (s^{-1})	N_1 (s^{-1})	σ (cm)	L (cm)	N_1/N_0	σ/L	k_cL	ω_c/N_0	ω_c/N_1	T_{obs}	T_{thy}
1b	0.50	1.11	0.43 (+0.06)	0.90	3.20	0.38	0.28	0.93	0.45	1.17	0.68	0.52
1c	0.50	1.16	0.46 (+0.01)	1.00	5.95	0.40	0.17	1.66	0.43	1.08	0.28	0.27
1d	0.50	1.20	0.34 (+0.01)	1.35	7.75	0.28	0.17	2.08	0.42	1.49	0.14	0.08
2b	0.51	1.40	0.42 (+0.07)	0.80	3.25	0.30	0.25	0.77	0.36	1.21	0.36	0.53
2c	0.51	1.40	0.33 (+0.09)	0.75	3.15	0.24	0.24	0.74	0.36	1.52	0.39	0.51
2d	0.51	1.51	0.00 (+0.31)	1.65	6.30	0.0	0.26	1.38	0.34	$\gg 1$	0.18	0.23
2e	0.51	1.55	0.06 (+0.14)	1.75	8.45	0.04	0.21	1.80	0.33	8.27	0.07	0.09
3b	0.47	1.38	0.27 (+0.20)	1.10	3.50	0.20	0.31	1.88	0.34	1.73	0.09	0.49
3c	0.47	1.41	0.18 (+0.14)	1.55	6.20	0.13	0.25	3.24	0.33	2.64	0.04	0.16
3d	0.47	1.48	0.00 (+0.31)	1.55	8.15	0.0	0.19	4.08	0.32	$\gg 1$	0.04	0.06
4b	0.52	1.43	0.40 (+0.13)	1.40	4.75	0.28	0.29	2.71	0.36	1.30	0.21	0.47
4c	0.52	1.52	0.36 (+0.05)	1.60	7.55	0.23	0.21	4.05	0.34	1.46	0.07	0.11
4d	0.51	1.60	0.00 (+0.19)	1.80	8.95	0.0	0.20	4.47	0.32	$\gg 1$	0.02	0.02
5b	0.52	1.48	0.52 (+0.06)	1.30	5.20	0.35	0.25	2.86	0.35	1.00	0.22	0.62
5c	0.52	1.53	0.27 (+0.10)	1.60	6.95	0.18	0.23	3.71	0.34	1.92	0.11	0.08
5d	0.52	1.60	0.18 (+0.10)	2.00	9.30	0.11	0.22	4.74	0.32	2.88	0.04	0.04
6b	0.52	1.43	0.26 (+0.28)	1.35	3.80	0.18	0.36	2.17	0.36	2.02	0.18	0.55
6c	0.52	1.52	0.45 (+0.06)	1.80	7.55	0.29	0.24	4.07	0.34	1.17	0.06	0.38
6d	0.52	1.57	0.14 (+0.08)	1.65	8.48	0.09	0.19	4.40	0.33	3.77	0.03	0.02

predict the proportion of energy that transmits through the mixed region to the strongly stratified region below. The results may be compared with the measured relative energy associated with the beam that transmits below the mixed region.

Specifically, snapshots of the filtered N_t^2 wave field are taken once the primary beam has reached steady state. For the oscillating cylinder experiments, steady state is reached after four buoyancy periods (less than 30 s). Horizontal slices are taken through the snapshot above and below the mixed region at $z_u+\sigma$ and $z_l-\sigma$, respectively. Taking these slices a distance σ away from the mixed region ensures that an unobstructed signal of the wave structure is captured, as shown in Fig. 8. Fourier series of these horizontal slices are taken, obtaining a sequence of amplitudes A_{In} and A_{Tn}, respectively, above and below the mixed region for each wave number $k_n=n2\pi/L_x$, in which L_x is the horizontal extent of the image's field of view.

An example of this procedure is shown in Fig. 8. A horizontal slice of the N_t^2 snapshot above the mixed region is taken at $z_u+\sigma=-8.20$ cm$+0.90$ cm$=-7.30$ cm and a horizontal slice below the mixed region is taken at $z_l-\sigma=-11.40$ cm-0.90 cm$=-12.30$ cm, where $z=0$ is the center of the cylinder. A Fourier series in the x-direction is performed on both slices resulting in a plot of Fourier amplitudes $A_n=A_{N_t^2}(k_n)$ for plane waves with discrete horizontal wave numbers, k_n. In the particular instance shown in Fig. 8(a), the upward-propagating beam from the cylinder reflects from the surface and partially interferes with the primary downward-propagating beam from the cylinder. However, windowing the time series to remove the secondary beam, we find this negligibly changes the magnitude of the Fourier amplitudes.

From the incident amplitudes, the predicted relative energy transmission is given by Eq. (17) with $A_n=A_{In}$. Separately, we measure the relative energy transmission as

$$T_{\text{obs}}=\frac{\sum_n \frac{1}{k_n^2}|A_{Tn}|^2}{\sum_n \frac{1}{k_n^2}|A_{In}|^2}. \tag{19}$$

The comparison of results is presented in Sec. IV.

IV. RESULTS

We begin by showing the results of experiment 1b in which a cylinder with radius $R=2.43$ cm oscillates vertically at a frequency $\omega_c=0.50$ s^{-1} and half-peak-to-peak amplitude $A=0.43$ cm. The density and N^2 profile is that shown in Fig. 5. Note that $\omega_c^2\approx 0.25\gtrsim N_1^2$, so partial reflection and transmission is anticipated. Figures 7 and 8 show corresponding Hilbert-filtered images and the discrete amplitude spectrum of the incident and transmitted waves.

The amplitudes and horizontal wave numbers from the upper (incident) and lower (transmitted) horizontal slices are used to calculate the experimental transmission coefficient of

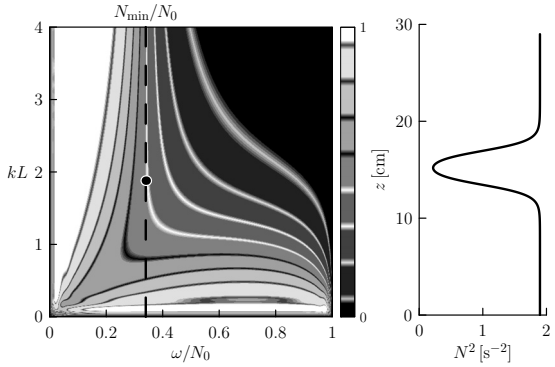

FIG. 9. Grayscale contours of the theoretical transmission coefficient (left) as a function of k and ω for the background N^2 profile (right) of experiment 3b. The black circle on the transmission plot indicates the theoretical transmission coefficient for this experiment, where $\omega=\omega_c$ and $k=k_c$. The vertical dashed line indicates $\omega=N_{\min}$, the minimum value of $N(z)$. Here, $N_{\min}=0.34N_0 \gg N_1=0.20N_0$ and $\omega_c=1.0N_{\min}=1.73N_1$.

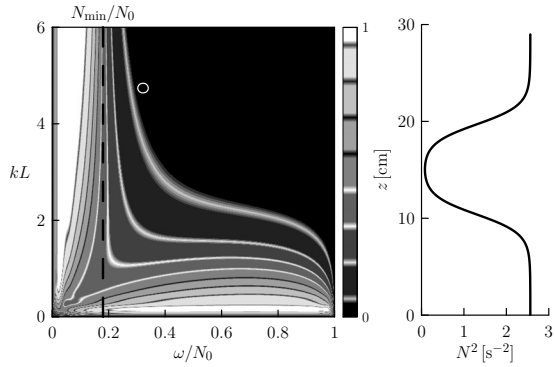

FIG. 10. As in Fig. 9 except showing the theoretical transmission coefficient and N^2 profile for experiment 5d. Here, $N_{\min}=0.18N_0 \gg N_1=0.11N_0$ and $\omega_c=1.8N_{\min}=2.88N_1$.

the beam from Eq. (19). In the case of experiment 1b, 68% of the incident energy was observed to pass through the mixed region.

The theoretical wave beam transmission coefficient based on the upper slice alone was calculated using Eq. (17), in which the corresponding transmission coefficients T_n were calculated numerically for each k_n and with ω_c constant. The prediction of 52% transmission in the case of experiment 1b is moderately smaller than the observed transmission coefficient.

The parameters and transmission coefficients for the experiments (with sets labeled 1–6) are listed in Table I. Successive intrusions are launched between different experiments within a particular set. The first experiment in a set (labeled "a") has uniform stratification. As expected, the waves propagated along a straight line with no partial reflection evident and so these trivial results are not shown in the table. In successive experiments within a set (sublabeled "b," "c," etc.), the mixed layer depth L becomes progressively larger with the exception of experiments 2b and 2c, for which no intrusion was launched between experiments.

In the oscillating cylinder experiments, the horizontal wave number spectrum of the incident wave typically peaks around a characteristic value

$$k_c \approx \frac{2\pi}{4R}\cos\Theta, \tag{20}$$

consistent with theory.[24]

In each set the cylinder radius and wave frequency are fixed. Hence the characteristic horizontal wave number k_c given by Eq. (20) is fixed. Therefore the parameter k_cL increases between successive experiments and the transmission coefficient is expected to decrease. This is indeed the case, as shown in the last two columns of Table I.

Although in most cases the theoretical transmission prediction agrees well with experiments, some of the results reveal significant discrepancies. We focus on three specific experiments to explain the origin of the discrepancies.

Consider experiment 3b, in which the observed transmission is much smaller than the theoretical prediction. For moderately large k_cL, the transmission varies rapidly with ω/N_0 when ω_c is close to $N_{\min}$. This is shown in Fig. 9, which plots the theoretical transmission coefficients for a range of ω and k for this experiment. The theoretical transmission coefficient $T_{\text{thy}}=0.49$ occurs at $\omega_c/N_0=0.34$ and $k_cL\approx 1.88$, as indicated by the black dot in Fig. 9. The figure shows that a small error in the experimental measurement of N_1 gives rise to large changes in the predicted transmission coefficient. Indeed, because $\sigma\simeq 0.3L$ the minimum value of $N(z)$ determined from the graph on the right-hand side of Fig. 9 is 70% larger than the measured value N_1 used to compute the N^2 profile. This moderate overestimate of the stratification of the mixed region results in a significant overprediction of the transmission coefficient from the observed value of $T_{\text{obs}}=0.09$.

Although in experiment 5d there is a large discrepancy between the minimum value of $N(z)$ and the measured value of N_1, the experimental and theoretical transmissions are relatively low and are in good agreement. The reason is evident in Fig. 10, which shows a plot of theoretical transmission coefficients for a range of ω and k for this experiment. At the cylinder frequency and characteristic wave number k_c, the theoretical transmission coefficient is $T_{\text{thy}}=0.04$. The value is small because the waves are significantly evanescent in the tunneling region. The frequency and wave number themselves lie well away from the transition region so the transmission coefficient does not vary significantly with errors in the measurement of N. Thus there is little difference between the predicted and measured value $T_{\text{obs}}=0.04$.

Finally we consider experiment 1c, whose experimental and theoretical transmissions are relatively high and are in good agreement. Figure 11 shows a plot of theoretical transmission coefficients for a range of ω and k for this experiment. The theoretical transmission coefficient $T_{\text{thy}}=0.27$ occurs for $N_1 \lesssim \omega_c \lesssim N_{\min}$, which is near the transition region. Although the predicted transmission is sensitive to errors, in this case the minimum value of N and the value of N_1 differ by less than 0.01 s^{-2}. Thus the prediction well matches the measured transmission of $T_{\text{obs}}=0.28$.

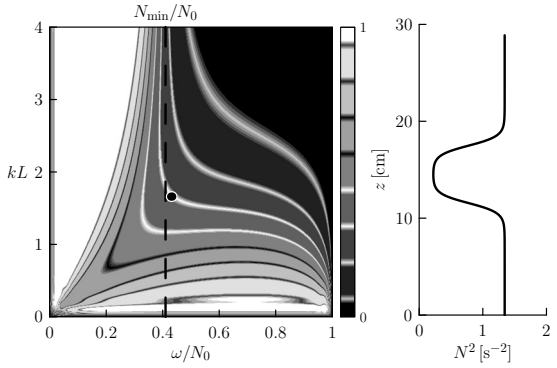

FIG. 11. As in Fig. 9 except showing the theoretical transmission coefficient and N^2 profile for experiment 1c. Here, $N_{min}=0.41N_0 \simeq N_1$ and $\omega_c=1.08N_1$.

V. DISCUSSION AND CONCLUSIONS

Internal wave beam tunneling through a weakly stratified layer was studied through the analysis of laboratory data and compared with an adaptation of existing theory. Internal waves were generated by a vertically oscillating cylinder producing a cross-pattern of wave beams. Experimental transmission coefficients were measured explicitly by finding the amplitudes of the plane waves of the beam above and below the mixed region. Theoretical transmission coefficients were computed using a numerical code that separately determined the transmission of the plane wave components associated with a wave beam. We found that the transmission coefficient is sensitive to small measurement errors in the background buoyancy frequency if the mixed region was sufficiently deep ($k_cL \gtrsim 2$) and the wave frequency was close to the minimum buoyancy frequency of the weakly stratified region.

The results have important consequences for predicting the evolution of internal waves generated by localized sources in the atmosphere. For example, internal waves generated by penetrative convection at thundercloud tops are frequently observed to be quasimonochromatic with frequencies comparable to the buoyancy frequency of the mesosphere,[16,17,30] Likewise, flow over isolated topography creates quasimonochromatic internal waves whose frequency is set by the background flow speed at ground level and the characteristic horizontal extent of the hill. Ducted internal waves are trapped in a layer outside of which their Doppler-shifted frequency is greater than the local buoyancy frequency. If they are evanescent far from the layer in which they are trapped, they are said to be strongly ducted. In a leaky duct, the depth of the evanescent region is comparable to or smaller than the horizontal wavelength of waves in the duct and above this evanescent region, the relative wave frequency is sufficiently small once more so the waves can propagate. This circumstance has been examined using Fourier-ray tracing methods[6,31] applied particularly to the study of internal waves generated by Jan Mayen Island. In this case, the waves had characteristic frequency and wave number that put them in the transition region where the transmission coefficient changes rapidly with small changes in wave frequency. Because atmospheric observations are likely not taken directly at the location of an observed leaky duct, the estimate of N^2 would differ from the actual *in situ* profile. Therefore, estimates of the rate at which energy escapes from the duct could be wrong by an order of magnitude.

The same conclusion holds for studies of internal wave tunneling between the seasonal and main thermocline in the ocean: the ability to predict accurately the energy transport by incident downward-propagating waves would be poor if the wave frequency is comparable to the minimum buoyancy frequency between the thermoclines. Because measurements of the density profile in the ocean are sparse, predictions of energy transfer can be considered accurate only if the waves have characteristic frequencies and wave numbers lying outside the transition region. Internal waves generated by surface processes are not so well understood as the generation of monochromatic wave beams by tidal flow over bottom topography. The frequency of the latter, being close to the Coriolis frequency, is so much smaller than the minimum of N between the seasonal and main thermocline that the waves lie well outside the transition region. However, recent studies have shown that Langmuir circulations[32] and the collapse of mixed regions[33] generate downward-propagating internal waves with a relatively narrow frequency band moderately below the local buoyancy frequency. Assessing whether or not these waves are able to propagate into the abyss requires careful assessment of the ambient conditions.

ACKNOWLEDGMENTS

The authors would like to thank Kerianne Yewchuk, who set up some of the experiments reported here. We also acknowledge the constructive comments of the reviewers who, in particular, helped improve the presentation of information in Figs. 1 and 2. This work has been supported by funding from the Canadian Foundation for Climate and Atmospheric Sciences (CFCAS).

[1] M. J. Lighthill, *Waves in Fluids* (Cambridge University Press, Cambridge, 1978).
[2] D. Broutman, J. W. Rottman, and S. D. Eckermann, "Ray methods for internal waves in the atmosphere and ocean," Annu. Rev. Fluid Mech. **36**, 233 (2004).
[3] F. P. Bretherton, "The propagation of groups of internal gravity waves in a shear flow," Q. J. R. Meteorol. Soc. **92**, 466 (1966).
[4] D. Broutman and W. R. Young, "On the interaction of small-scale oceanic internal waves with near-inertial waves," J. Fluid Mech. **166**, 341 (1986).
[5] D. Broutman and J. W. Rottman, "A simplified Fourier method for computing the internal wavefield generated by an oscillating source in a horizontally moving, depth-dependent background," Phys. Fluids **16**, 3682 (2004).
[6] D. Broutman, S. D. Eckermann, and J. W. Rottman, "Practical application of two-turning-point theory to mountain-wave transmission through a wind jet," J. Atmos. Sci. **66**, 481 (2009).
[7] J. C. Vanderhoff, K. K. Nomura, J. W. Rottman, and C. Macaskill, "Doppler spreading of internal gravity waves by an inertia-wave packet," J. Geophys. Res. **113**, C05018, doi:10.1029/2007JC004390 (2008).
[8] G. L. Brown, A. B. G. Bush, and B. R. Sutherland, "Beyond ray tracing for internal waves. Part II: Finite-amplitude effects," Phys. Fluids **20**, 106602 (2008).
[9] B. R. Sutherland and K. Yewchuk, "Internal wave tunneling," J. Fluid Mech. **511**, 125 (2004).
[10] J. T. Nault and B. R. Sutherland, "Internal wave tunneling across a mixed region," Phys. Fluids **19**, 016601 (2007).
[11] G. L. Brown and B. R. Sutherland, "Internal wave tunneling through non-uniformly stratified shear flow," Atmos.-Ocean. **45**, 47 (2007).

[12]M. Mathur and T. Peacock, "Internal wave beam propagation in nonuniform stratifications," J. Fluid Mech. **639**, 133 (2009).
[13]C. Eckart, "Internal waves in the ocean," Phys. Fluids **4**, 791 (1961).
[14]D. C. Fritts and L. Yuan, "An analysis of gravity wave ducting in the atmosphere: Eckart's resonances in thermal and Doppler ducts," J. Geophys. Res. **94**, 18455, doi:10.1029/JD094iD15p18455 (1989).
[15]Y. Yamada, H. Fukunishi, T. Nakamura, and T. Tsuda, "Breaking of small-scale gravity waves and transition to turbulence observed in OH airglow," Geophys. Res. Lett. **28**, 2153, doi:10.1029/2000GL011945 (2001).
[16]R. L. Walterscheid, G. Schubert, and D. G. Brinkman, "Small-scale gravity waves in the upper mesosphere and lower thermosphere generated by deep tropical convection," J. Geophys. Res. **106**, 31825, doi:10.1029/2000JD000131 (2001).
[17]J. B. Snively and V. P. Pasko, "Breaking of thunderstorm-generated gravity waves as a source of short-period ducted waves at mesopause altitudes," Geophys. Res. Lett. **30**, 2254, doi:10.1029/2003GL018436 (2003).
[18]P. G. Drazin and W. H. Reid, *Hydrodynamic Stability* (Cambridge University Press, Cambridge, 1981).
[19]M. Mathur and T. Peacock, "Internal wave interferometry," Phys. Rev. Lett. **104**, 118501 (2010).
[20]Y. V. Kistovich and Y. D. Chashechkin, "Linear theory of the propagation of internal wave beams in an arbitrarily stratified liquid," J. Appl. Mech. Tech. Phys. **39**, 729 (1998).
[21]G. Oster, "Density gradients," Sci. Am. **213**, 70 (1965).
[22]D. E. Mowbray and B. S. H. Rarity, "A theoretical and experimental investigation of the phase configuration of internal waves of small amplitude in a density stratified liquid," J. Fluid Mech. **28**, 1 (1967).
[23]B. Voisin, "Internal wave generation in uniformly stratified fluids. Part 2. Moving point sources," J. Fluid Mech. **261**, 333 (1994).
[24]D. G. Hurley and G. Keady, "The generation of internal waves by vibrating elliptic cylinders. Part 2: Approximate viscous solution," J. Fluid Mech. **351**, 119 (1997).
[25]B. R. Sutherland, S. B. Dalziel, G. O. Hughes, and P. F. Linden, "Visualisation and measurement of internal waves by 'synthetic schlieren.' Part 1: Vertically oscillating cylinder," J. Fluid Mech. **390**, 93 (1999).
[26]B. R. Sutherland, "Interfacial gravity currents. I. Mixing and entrainment," Phys. Fluids **14**, 2244 (2002).
[27]V. Croquette and H. Williams, "Nonlinear waves of the oscillatory instability on finite convective rolls," Physica D **37**, 300 (1989).
[28]N. B. Garnier, A. Chiffaudel, F. Daviaud, and A. Prigent, "Nonlinear dynamics of waves and modulated waves in 1D thermocapillary flows. I. General presentation and periodic solutions," Physica D **174**, 1 (2003).
[29]M. J. Mercier, N. B. Garnier, and T. Dauxois, "Reflection and diffraction of internal waves analyzed with the Hilbert transform," Phys. Fluids **20**, 086601 (2008).
[30]R. L. Walterscheid, J. H. Hecht, R. A. Vincent, I. M. Reid, J. Woithe, and M. P. Hickey, "Analysis and interpretation of airglow and radar observations of quasi-monochromatic gravity waves in the upper mesosphere and lower thermosphere over Adelaide, Australia," J. Atmos. Sol.-Terr. Phys. **61**, 461 (1999).
[31]S. D. Eckermann, D. Broutman, J. Ma, and J. Lindeman, "Fourier-ray modeling of short-wavelength trapped lee waves observed in infrared satellite imagery near Jan Mayen," Mon. Weather Rev. **134**, 2830 (2006).
[32]J. A. Polton, J. A. Smith, J. A. MacKinnon, and A. E. Tejada-Martinez, "Rapid generation of high-frequency internal waves beneath a wind and wave forced oceanic surface mixed layer," Geophys. Res. Lett. **35**, L13602, doi:10.1029/2008GL033856 (2008).
[33]B. R. Sutherland, A. N. F. Chow, and T. P. Pittman, "The collapse of a mixed patch in stratified fluid," Phys. Fluids **19**, 116602 (2007).